INITIAL PULSE-ECHO IMAGING RESULTS WITH ONE-DIMENSIONAL CAPACITIVE MICROMACHINED ULTRASONIC TRANSDUCER ARRAYS

Ö. Oralkan, X. C. Jin, K. Kaviani, A. S. Ergun, F. L. Degertekin*, M. Karaman and B. T. Khuri-Yakub

Edward L. Ginzton Laboratory, Stanford University, Stanford, CA 94305-4085

*Woodruff School of Mechanical Engineering, Georgia Institute of Technology, Atlanta, GA 30332

Abstract— **In this paper, the first experimental results of pulse-echo imaging employing a 1-D capacitive micromachined ultrasonic transducer array are presented. A 1-D array consisting of 16 elements is used in the experiment. A wire phantom consisting of seven steel wires immersed in vegetable oil is used as the imaging target. A B-scan image with a sector angle of 90 degrees and an image depth of 150 mm is reconstructed by employing RF beamforming and synthetic phase array approaches. The reconstructed image is displayed at different display dynamic ranges. The measured near and far side lobe levels are around -25 dB and -35 dB, respectively. The noise floor of the image is below -50 dB.**

Keywords— **Ultrasonic transducer, 1-D array, capacitive micromachined transducer, beamforming, medical ultrasound imaging**

I. Introduction

In recent years, capacitive micromachined ultrasonic transducers (cMUTs) have emerged as an attractive alternative to conventional piezoelectric transducers [1], [2] . The cMUTs provide advantages in ease of fabrication, size reduction, low self-noise and potential for electronic integration in addition to their performance attributes such as bandwidth and sensitivity. Fabrication of 1-D and 2-D cMUT arrays and interconnects are quite simple and straightforward compared with piezoelectric transducer arrays. The fabrication process for cMUTs is fully compatible with standard integrated circuit fabrication processes. As a result, cMUT arrays can be integrated with custom electronics, either on chip or as a three-dimensional multi-chip module [3] .

The fabrication process for cMUTs has been reported earlier [4]. The equivalent circuit model has also been proposed [5] and the validity of the model has been confirmed by experimental results [6]. First imaging results using cMUTs were basically demonstrating images based on reception from an active source located at a distance from a cMUT array [7]. This paper demonstrates the first pulse-echo B-scan sector imaging using a 1-D cMUT array.

The aim of this paper is to present the preliminary pulse-echo imaging results using 1-D cMUT arrays to demonstrate the viability of cMUTs for ultrasound imaging, especially for medical applications such as diagnosis and guidance. The paper gives a brief outline of cMUTs and 1-D cMUT arrays. The experimental setup and methods are explained. Image reconstruction procedure is described and reconstructed B-scan images are presented. A quantitative analysis of the results is also included.

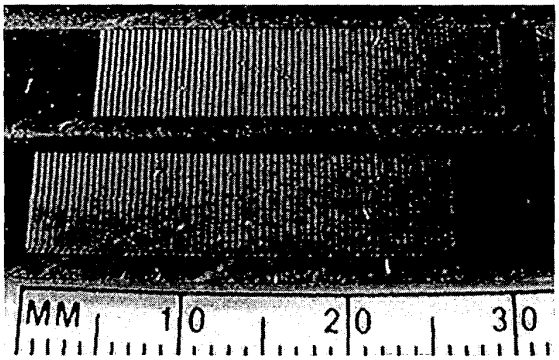

Fig. 1. Top view of two 64-element 1-D cMUT arrays.

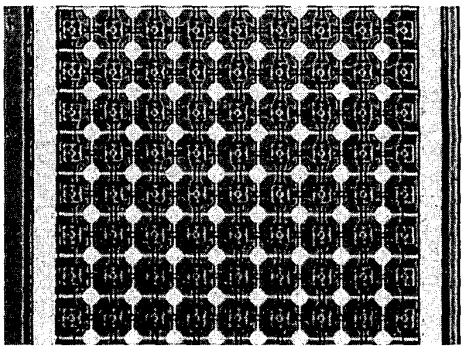

Fig. 2. Magnified view of a single 1-D array element.

II. 1-D cMUT Arrays

An element in a 1-D linear cMUT array consists of many small capacitor cells connected in parallel. A top view of 64-element 1-D cMUT arrays is shown in Fig. 1. The small capacitor cells forming a single element can be seen in Fig. 2 where a portion of the 1-D array element is shown. A cMUT cell consists of a metalized membrane (top electrode) suspended above a heavily doped silicon substrate (bottom electrode). In operation of cMUTs, a DC voltage is placed between the metalized membrane and the substrate. The membrane is attracted toward the bulk and stress within the membrane resists the attraction. Ultra-

0-7803-6365-5/00/$10.00

TABLE I

PHYSICAL PARAMETERS OF THE 1-D CMUT ARRAY.

height of an element	$5.6mm$
width of an element	$280\mu m$
element pitch	$400\mu m$

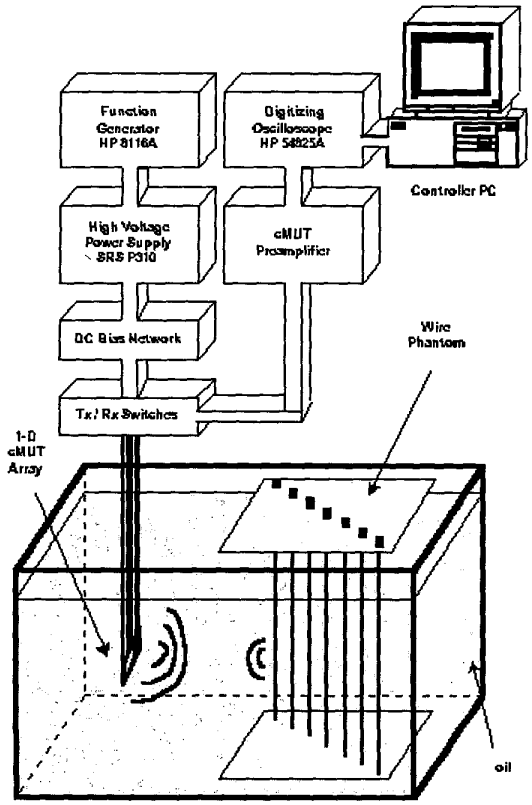

Fig. 3. Experimental setup.

sound is generated by driving the membrane with an alternating voltage. If the biased membrane is subjected to ultrasound, detection currents are generated.

The physical dimensions of the 1-D cMUT array used in this work are listed in Table I. A single 1-D array element in this case consists of 1280 parallel connected capacitor cells.

III. EXPERIMENTAL PULSE-ECHO IMAGING

In this experiment, a 16-element portion of a 64-element 1-D cMUT array is used to generate ultrasound and receive echo signals. In this study, a 16-element array is chosen particularly to reduce data acquisition time and complexity. As the imaging target, a phantom consisting of seven steel wires is used, each having a diameter of 0.5 mm. The location of wires is arranged in a diagonal fashion, so that the point spread functions (PSF) at different spatial locations can be measured. The wire phantom and the cMUT

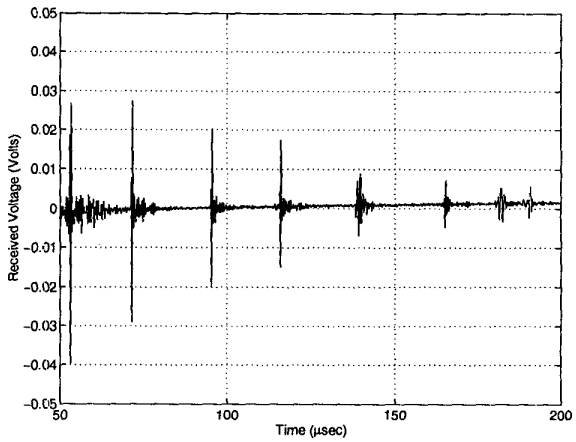

Fig. 4. Echo signal received by the second element in the array when the first one is transmitting.

array are immersed into vegetable oil.

In the experiment, the DC bias voltage on the cMUT array is set to 50 V and a 10 V, 100 ns rectangular pulse is applied to generate ultrasound signals. One element is used to transmit ultrasound signals, and one element is used to listen to echo signals at a time. The experimental setup is depicted in Fig. 3. The echo signals received by the array elements are amplified by the preamplifier. The amplified signal is sampled at a rate of 25 MHz and digitized with a resolution of 8-bits by a digitizing oscilloscope. The digitized signals for all transmit-receive pairs are stored for further processing.

Figure. 4 shows the echo signal received by the second element in the array when the first element is transmitting. The echo signals coming from seven different wires in the phantom are clearly identified in the figure. The echo signal coming from the third wire is depicted in Fig. 5. The long ring-down time following the main echo signal in this figure is an indication of crosstalk between array elements. Previously, it has been reported that Lamb waves propagating in the silicon wafer and Stoneley-type waves propagating at the fluid-silicon wafer interface are the major reasons for the crosstalk between array elements.

The pulse-echo frequency response, Fourier transform of a single A-scan signal associated with the third wire, is shown in Fig. 6. This pulse-echo frequency response is centered around 2.3 MHz with a fraction bandwidth of 80%. It has been previously shown that cMUTs have a fractional bandwidth of more than 100%. In this case, the frequency response shown in Fig. 6 includes the effects of frequency dependent attenuation in oil and frequency shaping of electronics. The crosstalk between array elements also cause distortion and ripples at some frequencies in the pulse-echo frequency response. Currently, the acoustic coupling mechanisms and the crosstalk reduction techniques are subjects of extensive research.

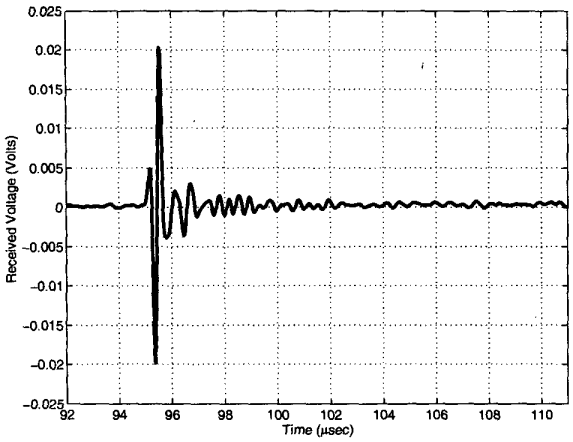

Fig. 5. Echo signal from the third wire.

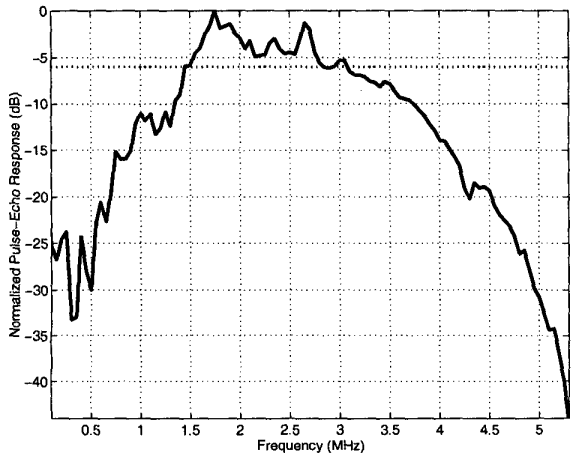

Fig. 6. Pulse-echo frequency response.

IV. Image Reconstruction

Once the complete data set for all transmit-receive combinations of array elements is obtained, the digitized raw RF A-scan data are processed digitally on a computer to reconstruct the B-scan sector image (Fig. 7). First, a digital band-pass filter is applied on the raw data to eliminate the out-of-band noise. The filtered signals are upsampled by a factor of four to decrease the effects of delay quantization. Afterwards, the differences in magnitude of echo signals associated with different depths are compensated by applying a variable gain amplification on A-scans. In Fig. 4, it can be seen that the difference between uncompensated echo signals can be as large as 20 dB. The image is reconstructed by employing RF beamforming and synthetic phased array approaches [8], [9]. In beamforming, first, the image sector plane is sampled uniformly in the axial direction and uniformly in $\sin(\theta)$ in the angular direction. To reconstruct the gold standard image using the cMUT array, dynamic focusing is employed both in transmit and receive. A minimum $f_{\#}$ of 2 is used. The array is not apodized (rect-

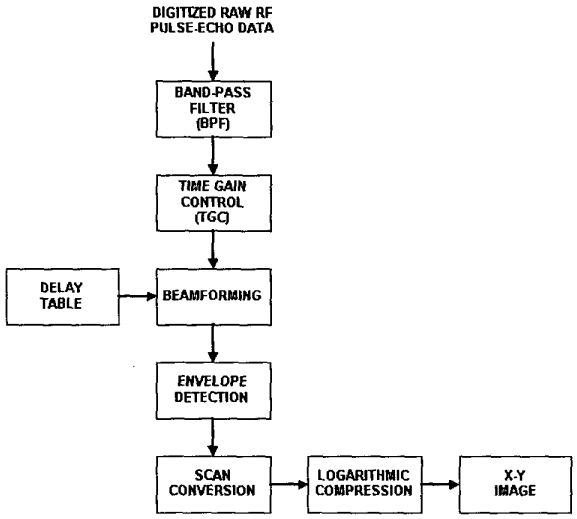

Fig. 7. Image reconstruction steps.

angular aperture function) both in transmit and receive. After coherent image formation is completed, the envelope of the resulting image is detected. Finally, the image scans are converted from polar to cartesian coordinates by using bilinear interpolation. The final reconstructed B-scan sector image with 150 mm image depth and 90 degrees sector angle is displayed at 20, 30, and 40 dB dynamic display ranges in Fig. 8.

V. Analysis of Results

The image shown in Fig. 8a has no sidelobes visible at a 20 dB dynamic display range. In the image with 30 dB dynamic range, the near side lobes become visible, indicating that the near side lobe level is between -20 dB and -30 dB. Further, looking at the image with 40 dB dynamic range, it can be seen that the far side lobe level is between -30 dB and -40 dB. The electronic noise floor of the reconstructed image is below -50 dB, and thus not visible.

For further analysis of side lobe levels and 3-dB beamwidth, the lateral extent of the fifth wire image at 104 mm, representing the lateral PSF, is presented in Fig. 9. In this figure, the near and far side lobe levels are measured as -25 dB and -35 dB, respectively. The full angular spread between the 3-dB points ($\Delta\theta_{3dB}$) for the given PSF is measured as 0.1 radians which is in good agreement with the theoretical value obtained as:

$$\Delta\theta_{3dB} = \frac{0.89\lambda}{\pi D cos(\theta_i)}, \quad (1)$$

where λ, D, and θ_i correspond to wavelength, array size, and steering angle, respectively [10].

In Fig. 9, it can be observed that the simulated and measured PSF are in good agreement except the higher side lobes in the measured PSF. Currently, this difference is presumed to be a result of crosstalk between array elements. The modeling of acoustic coupling and its effects on final images are under investigation.

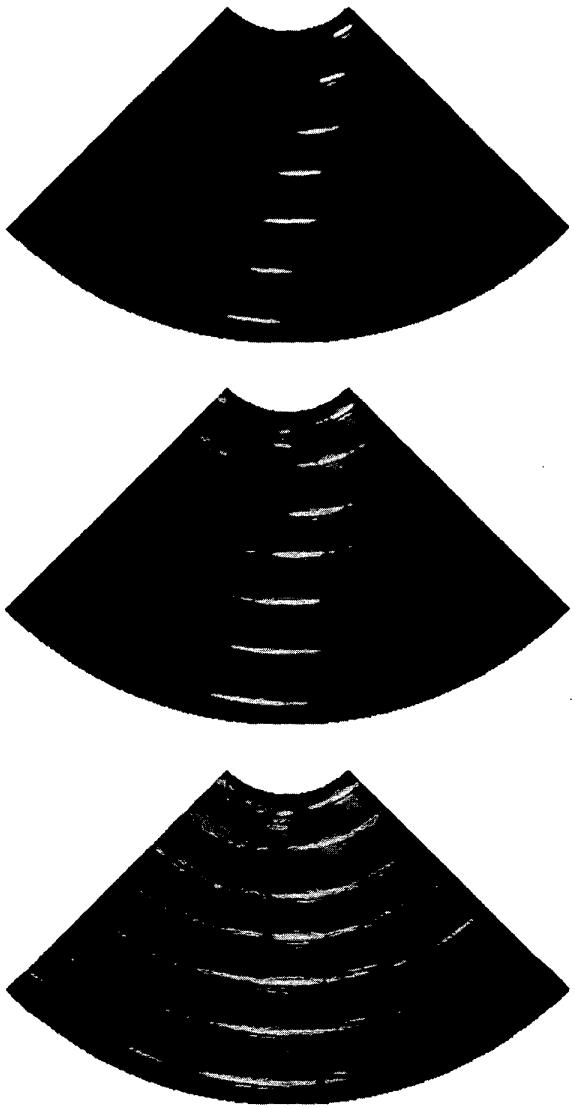

Fig. 8. Reconstructed B-scan sector images. From top to bottom, with dynamic display ranges of 20 dB, 30dB, and 40dB

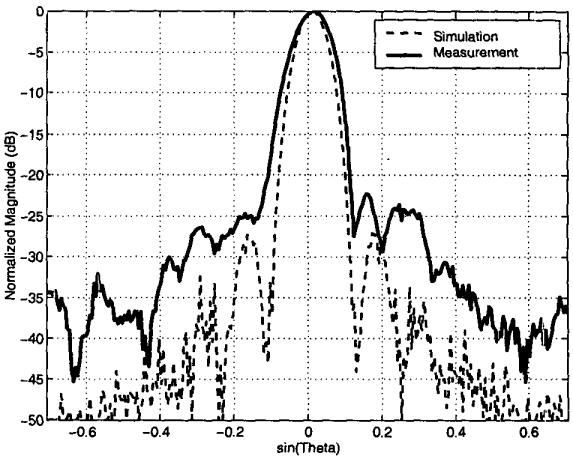

Fig. 9. Point spread function at 104mm.

VI. Conclusion

In this paper, the first experimental results of pulse-echo imaging using 1-D cMUT arrays are successfully demonstrated. The wide-band feature and the sensitivity of cMUTs reported in our previous publications are confirmed through the experimental pulse-echo imaging explored here.

To improve the performance of cMUT arrays further, extensive research will be carried on crosstalk reduction, receive sensitivity optimization, and maximizing transmit power.

Our experimental studies on pulse-echo imaging using 64 and 128 element 1-D cMUT arrays and 16x16 2-D cMUT arrays are in progress. System level research is conducted for the realization of a volumetric scanner for image guided surgery using 2-D cMUT arrays.

Acknowledgments

This work was supported by the Office of Naval Research.

References

[1] M. I. Haller and B. T. Khuri-Yakub, "A surface micromachined electrostatic ultrasonic air transducer," in *Ultrasonics Symposium*, Cannes, France, 1994, pp. 1241-1244.

[2] Eccardt, P., Niederer, K., Scheiter, T., and Hierold, C., "Surface micromachined ultrasound transducers in CMOS technology," in *Ultrasonics Symposium*, San Antonio, Texas, 1996, pp. 959–962.

[3] X. C. Jin, S. Calmes, C. H. Cheng, F. L. Degertekin, and B. T. Khuri-Yakub, "Micromachined capacitive ultrasonic immersion transducer array," in *Transducers'99, Sendai, Japan, 1999.*

[4] X. C. Jin, I. Ladabaum, and B. T. Khuri-Yakub, "The microfabrication of capacitive ultrasonic transducers," *IEEE/ASME J. Microelectromech. Syst.*, vol. 7, pp. 295-302, Sep 1998.

[5] I. Ladabaum, X. C. Jin, H. T. Soh, A. Atalar, and B. T. Khuri-Yakub, "Surface micromachined capacitive ultrasonic transducers," *IEEE Trans. Ultrason., Ferroelect., Freq. Contr.*, vol. 45, no. 3, pp. 678-689, May 1998.

[6] O. Oralkan, X. C. Jin, F. L. Degertekin, and B. T. Khuri-Yakub, "Simulation and experimental characterization of a 2-D capacitiv e micromachined ultrasonic transducer array element," *IEEE Trans. on Ultrason., Ferroelect., and Freq. Contr.*, vol. 46, no. 6, pp. 1337-1340, November 1999.

[7] X. C. Jin, F. L. Degertekin, S. Calmes, X. J. Zhang, I. Ladabaum, and B. T. Khuri-Yakub, "Micromachined capacitive transducer arrays for medical ultrasound imaging," in *Proc. IEEE Ultrason. Symp.*, Sendai, Japan, 1998, pp. 1877-1880.

[8] K. E. Thomenius, "Evolution of ultrasound beamformers," in *Proc. IEEE Ultrason. Symp.*, San Antonio, Texas, 1996, pp. 1615-1622.

[9] M. Karaman, P.-C. Li, and M. O'Donnell, "Synthetic aperture imaging for small scale systems," *IEEE Trans. on Ultrason., Ferroelect., and Freq. Contr.*, vol. 42, no. 3, pp. 429-442, May 1995.

[10] G. S. Kino, *Acoustic Waves: Devices, Imaging, and Analog Signal Processing.* Englewood Cliffs, NJ:Prentice-Hall, 1987.